Pergamon

Int. J. Heat Mass Transfer. Vol. 40, No. 10, pp. 2261–2272, 1997

0017–9310/97 $17.00+0.00

PII: S0017-9310(96)00320-1

Thermal performances of different shape porous blocks under an impinging jet

WU-SHUNG FU and HSIN-CHIEN HUANG

Department of Mechanical Engineering, National Chiao Tung University, Hsinchu, 30050, Taiwan, Republic of China

(*Received* 23 *April* 1996 *and in final form* 6 *September* 1996)

Abstract—A study of the enhancement of the convection heat transfer of a laminar slot jet impinging on a porous block mounted on a heated region was investigated numerically. A numerical method (SIMPLEC) was adopted to solve the governing equations, and a one-equation thermal model with Van Driest's wall function was considered for solving the energy equation. Three different shape porous blocks (rectangle, convex and concave) were studied. The results indicated that the heat transfer is mainly affected by a fluid flowing near the heated region. For a lower porous block, the heat transfer is enhanced by the three types of porous block. However, for a higher porous block, heat transfer is only enhanced by the concave porous block. © 1997 Elsevier Science Ltd. All rights reserved.

INTRODUCTION

Due to the importance of porous media in many thermal devices, the characteristics of the heat transfer performance of porous media have been investigated widely and deeply in the last decade.

Vafai and Kim [1] studied the thermal performance for a composite porous medium-fluid system. The porosity and the effective thermal conductivity were assumed to be constant. The enhancement of the thermal performance of the porous medium mainly depended on the ratio of the effective thermal conductivity of the porous medium to the fluid thermal conductivity. When the ratio was sufficiently greater than 1, enhancement of the thermal performance is obtained: otherwise, the heat transfer rate decreased. Huang and Vafai [2] studied the heat transfer of a flat plate mounted with a porous block array. The porosity ε was regarded as constant, and the channeling effect in the near-wall region and the thermal dispersion were both neglected. The porous block array in the external flow field significantly reduced the heat transfer rate on the flat plate as shown in the results. However, different trends in the internal flow field were obtained by Hadim [3]. He investigated two configurations: a fully porous channel and a partially divided porous channel. The results indicated that the partially divided porous channel configuration was an attractive heat transfer augmentation technique, although the ratio of the effective thermal conductivity of the porous medium to the fluid thermal conductivity was equal to 1. Huang and Vafai [4] indicated four effects (penetrating, blowing, suction and boundary layer separation) on the flow and thermal fields in a channel mounted with porous arrays. Hwang and Chao [5] conducted experiments and numerical methods to study the thermal performance of a porous channel, and the results illustrated that thermal enhancement could be obtained by using a high thermal conductivity porous medium. Fu *et al.* [6] investigated numerically the thermal performance of a porous block mounted on a partially heated wall in a laminar-flow channel. The results indicated that the thermal performance was enhanced for the partially blocked situation by using a porous block with a higher porosity and bead diameter: however, the results were opposite to those for the fully blocked situation.

Based upon previously mentioned literature, the conclusion that enhancement of the heat transfer performance of a porous medium occurs under certain conditions can be drawn. The fact that more fluid is forced to flow through a porous medium is important. To satisfy the above demand, an impinging jet, which can control the flow direction of fluids and enhance the heat transfer performance of an object impinged by the jet, may, after all, be an appropriate device. As for the investigation of the thermal characteristics of the impinging jet, there are a number of articles that have been published in the past.

Martin [7] briefly reviewed the early studies of jet impingement, including a single round jet, arrays of round jets, a single slot jet, and arrays of slot jets. Many empirical equations for heat and mass transfer coefficients were provided, based on experimental data. In addition, many studies of the jet impingement, such as those of Gardon and Akfirat [8, 9], Miyazaki and Silberman [10], Sparrow and Lee [11], and Jambunathan *et al.* [12], have specialized in the effects of parameters such as the Reynolds number, the jet-to-plate distance, and the velocity-inlet profile on the local and average Nusselt number. The results indicated that enhancement of the Nusselt number could be obtained by using a shorter jet-to-plate

NOMENCLATURE

b	width of slot jet [m]
B_o	coefficient of stagnant conductivity
C_f	specific heat of fluid [kJ kg^{-1} °C^{-1}]
d_p	porous bead diameter [m]
Da	Darcy number (K/b^2)
D_T	empirical constant in thermal dispersion conductivity
F	inertia factor
H_j	dimensional distance from jet inlet to the highest position of the porous block [m]
HJ	dimensionless distance from jet inlet to the highest position of the porous block (H_j/b)
H_p	dimensional height of porous block [m]
HP	dimensionless height of porous block (H_p/b)
H_{pc}	dimensional height of central region of porous block [m]
HP_c	dimensionless height of central region of porous block (H_{pc}/b)
H_{pr}	dimensional height of right-hand side of porous block [m]
HP_r	dimensionless height of right-hand side of porous block (H_{pr}/b)
H_z	dimensional distance from jet inlet to solid wall [m]
HZ	dimensionless distance from jet inlet to solid wall (H_z/b)
k_d	stagnant conductivity [W m^{-1} °C^{-1}]
k_e	effective thermal conductivity of porous block [W m^{-1} °C^{-1}]
k_f	thermal conductivity of fluid [W m^{-1} °C^{-1}]
k_s	thermal conductivity of solid phase in porous block [W m^{-1} °C^{-1}]
k_t	thermal dispersion conductivity [W m^{-1} °C^{-1}]
K	permeability [m^2]
l	Van Driest's wall function
L_p	dimensional length of the porous block
LP	dimensionless length of the porous block (L_p/b)
$\dot{m}$	dimensionless flow rate
$\overline{Nu}$	mean Nusselt number in the X-direction
p	dimensional pressure [N m^{-2}]
P	dimensionless pressure ($p/\rho v_o^2$)
Pr_f	Prandtl number of fluid in external flow field ($v_f\rho_f C_f/k_f$)
Pr_p	Prandtl number of fluid in porous media ($v_f\rho_f C_f/k_e$)
r_1, r_2	coefficients in equation (1)
Re	Reynolds number ($v_o b/v_f$)
Re_P	bead diameter based Reynolds number ($\lvert\vec{u}_p\rvert d_p/v_f$)
Δs	shortest distance from the calculated point to the boundaries of the porous block [m]
T	temperature [°C]
u	dimensional velocity in x-direction [m s^{-1}]
U	dimensionless velocity in x-direction (u/v_o)
v	dimensional velocity in y-direction [m s^{-1}]
v_o	jet inlet velocity [m s^{-1}]
V	dimensionless velocity in Y-direction (v/v_o)
x, y	dimensional Cartesian coordinates [m]
X, Y	dimensionless Cartesian coordinates (x/b, y/b).

Greek symbols

ψ	dimensionless stream function
ε	porosity [m^3 m^{-3}]
ε_e	effective porosity [m^3 m^{-3}]
Φ	computational variable
γ	shape factor
Λ	ratio of thermal conductivity of solid phase to fluid phase in porous block
μ	viscosity [kg m^{-1} s^{-1}]
ρ	fluid density [kg m^{-3}]
ν	kinematic viscosity
ω	empirical constant in Van Driest's wall function
θ	dimensionless temperature $[(T-T_o)/(T_w-T_o)]$.

Superscripts

n	the nth iteration index
—	mean value
→	velocity vector.

Subscripts

c	central line of porous block
CV	control volume
e	effective value
f	external flow field
o	inlet condition
p	porous media
r	right side of porous block
w	solid wall
wop	without-porous-block case.

Other

$\lvert\ \rvert$	magnitude of velocity vector.

distance, a higher Reynolds number, and a parabolic velocity profile of the inlet jet. Polat *et al.* [13] gave a comprehensive summary, including a laminar and turbulent jet impinging on a flat surface, of the numerical models. In their study, both the numerical models and the results were discussed in detail. In the above literature, the dimensions of the impingement plate were much larger than the width of the jet inlet. Hence, the impingement plate should be treated as an infinite plate. However, in many industrial applications, e.g. electronic cooling, this assumption is not always appropriate.

Consequently, the aim of this study is to investigate numerically the effects of a laminar jet on the heat transfer performance of different shape porous blocks mounted on a heated plate. In order to increase the fluid flow through the porous medium, the shape of the porous block except for the usually used rectangular shape, concave and convex shapes are taken into consideration. The effects of the ratios of the height of the porous block and the distance between the porous block and the jet to the width of the jet on the heat transfer performance are mainly investigated. However, other parameters, such as the Reynolds number, bead diameter ratio, porosity, and Prandtl number, are selected, based on the authors' previous study [6]. The results indicated that the thermal performance is mainly enhanced by more fluid flowing through the porous medium and near a heated region. For the concave shaped cases, the mean Nusselt numbers are enhanced. However, for the convex and rectangular shapes, the mean Nusselt numbers are enhanced for the lower porous blocks, but decreased for the higher porous ones. Generally, from the heat transfer point of view, the higher porous block is regarded as a barrier, and the thermal performance becomes worse.

PHYSICAL MODEL

The physical model is shown symmetrically in Fig. 1. There is a two-dimensional laminar slot jet impinging on a partially heated plate. The width of the jet inlet is b. The uniform inlet velocity and the temperature of the jet are v_o and T_o, respectively. Only a portion of the impinged plate is heated, the rest of the plate being insulated. The length of the heated region is L_p, which is equal to $2b$, and the temperature of the heated region is T_w, which is higher than T_o. A porous block is mounted on the heated part of the impinged plate. Three different types of porous block (rectangular, convex and concave) are chosen. The definitions of these three blocks [shown in Fig. 2(a)–(c)] are based on the comparison of the heights of the right-hand side (H_{pr}) and the central region (H_{pc}). It is defined for rectangular, convex and concave porous blocks as $H_{pc} = H_{pr}$, $H_{pc} \geqslant H_{pr}$ and $H_{pc} \leqslant H_{pr}$, respectively. The distances from the jet inlet to the highest position of the porous block and the impinged plate are H_j and H_z, respectively. The whole computation

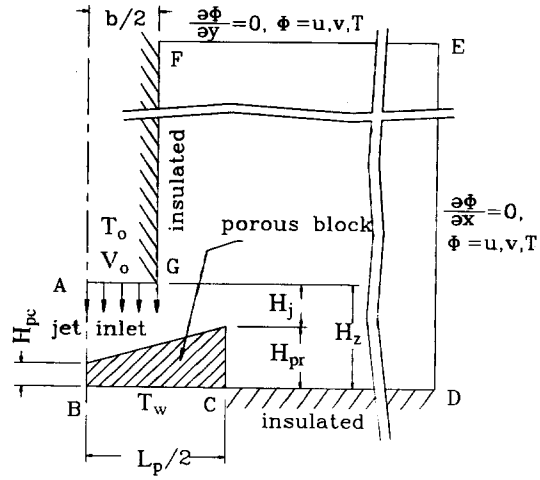

Fig. 1. Physical model.

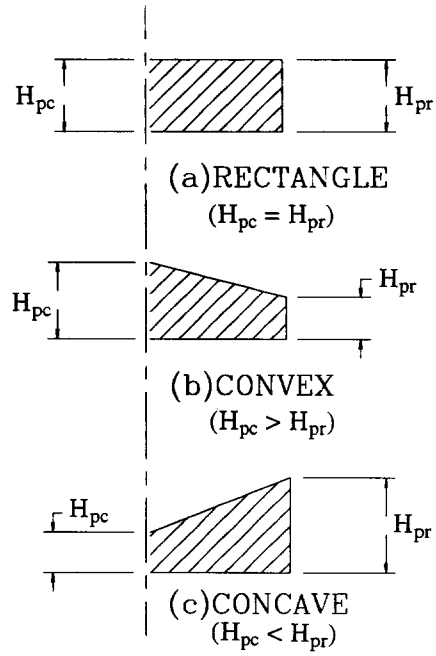

Fig. 2. Definitions of porous blocks: (a) rectangular, (b) convex, and (c) concave.

domain is large enough for fully developed distributions of the velocity and temperature to be formed. Under this configuration, the flow field can be decomposed into two conjugate regions: one stands for the internal flow field, which is bounded by the porous block; and the other is called the external flow field, which excludes the porous media.

In order to simplify the problem, some assumptions are made as follows:

(1) The porous block is made of spherical beads. It is non-deformable and does not chemically react with the fluid.

(2) The flow field is steady-state, two-dimensional, single-phase, laminar and incompressible.

(3) The fluid properties are constant and the effect of gravity is neglected.

(4) The transverse thermal dispersion is modeled by Van Driest's wall function [14]: hence, a one-equation model of the energy equation is used.

(5) The effective viscosity of the porous medium is equal to the viscosity of the external fluid.

(6) The profiles of the inclined surface of the convex and concave blocks are assumed to be straight lines.

The porosity ε, permeability K, and inertia factor F are defined as [15]

$$\varepsilon = \varepsilon_e(1+r_1 e^{-r_2 \Delta s/d_p}) \tag{1}$$

$$K = \frac{\varepsilon^3 d_p^2}{150(1-\varepsilon)^2} \tag{2}$$

$$F = \frac{1.75}{\sqrt{150}\varepsilon^{1.5}} \tag{3}$$

where Δs is the shortest distance from the calculated point to the boundary of the porous block, and r_1 and r_2 are both empirical constants.

The effective thermal conductivity of a porous medium (k_e) is a combination of the stagnant conductivity k_d and the thermal dispersion conductivity k_t [14], which simulates the transverse thermal dispersion. The relationship between k_e, k_d and k_t is then

$$k_e = k_d + k_t \tag{4}$$

and k_d is defined as

$$\frac{k_d}{k_f} = 1-\sqrt{1-\varepsilon}+\frac{2\Lambda\sqrt{1-\varepsilon}}{\Lambda-B_o} \times\left[\frac{B_o\Lambda(\Lambda-1)}{(\Lambda-B_o)^2}\ln\left(\frac{\Lambda}{B_o}\right) - \frac{B_o+1}{2} - \frac{\Lambda(B_o-1)}{\Lambda-B_o}\right] \tag{5}$$

where

$$\Lambda = \frac{k_s}{k_f} \tag{6}$$

$$B_o = 1.25\left(\frac{1-\varepsilon}{\varepsilon}\right)^{10/9} \tag{7}$$

and k_t is defined by Van Driest's wall function as

$$\frac{k_t}{k_f} = D_T\, Pr\, Re_p |\vec{u}_p| l \tag{8}$$

where D_T is an empirical constant, and Re_p is the bead diameter based Reynolds number, defined as

$$Re_p = \frac{|\vec{u}_p| d_p}{\nu_f} \tag{9}$$

and l is the Van Driest's wall function defined as

$$l = 1-e^{-\Delta s/\omega d_p} \tag{10}$$

where ω is an empirical constant.

Based on the above assumptions and with the consequent characteristics for b, $T_w - T_o$, ρv_o^2 and v_o, the governing equations, boundary conditions and geometry dimensions are normalized as follows:

(1) Governing equations of the external flow field

continuity equation

$$\frac{\partial U_f}{\partial X} + \frac{\partial V_f}{\partial Y} = 0 \tag{11}$$

X-momentum equation

$$U_f\frac{\partial U_f}{\partial X} + V_f\frac{\partial U_f}{\partial Y} = -\frac{\partial P_f}{\partial X} + \frac{1}{Re}\left(\frac{\partial^2 U_f}{\partial X^2} + \frac{\partial^2 U_f}{\partial Y^2}\right) \tag{12}$$

Y-momentum equation

$$U_f\frac{\partial V_f}{\partial X} + V_f\frac{\partial V_f}{\partial Y} = -\frac{\partial P_f}{\partial Y} + \frac{1}{Re}\left(\frac{\partial^2 V_f}{\partial X^2} + \frac{\partial^2 V_f}{\partial Y^2}\right) \tag{13}$$

energy equation

$$U_f\frac{\partial \theta_f}{\partial X} + V_f\frac{\partial \theta_f}{\partial Y} = \frac{1}{Re\, Pr_f}\left(\frac{\partial^2 \theta_f}{\partial X^2} + \frac{\partial^2 \theta_f}{\partial Y^2}\right) \tag{14}$$

(2) Governing equations of the internal flow field [16]

continuity equation

$$\frac{\partial U_p}{\partial X} + \frac{\partial V_p}{\partial Y} = 0 \tag{15}$$

X-momentum equation

$$U_p\frac{\partial}{\partial X}\left(\frac{U_p}{\varepsilon}\right) + V_p\frac{\partial}{\partial Y}\left(\frac{U_p}{\varepsilon}\right) = -\frac{\partial P_p}{\partial X} + \frac{1}{Re}\left(\frac{\partial^2 U_p}{\partial X^2} + \frac{\partial^2 U_p}{\partial Y^2}\right) - \frac{1}{Re\, Da}\varepsilon U_p - \frac{F|\vec{u}_p|}{\sqrt{Da}}\varepsilon U_p \tag{16}$$

Y-momentum equation

$$U_p\frac{\partial}{\partial X}\left(\frac{V_p}{\varepsilon}\right) + V_p\frac{\partial}{\partial Y}\left(\frac{V_p}{\varepsilon}\right) = -\frac{\partial P_p}{\partial X} + \frac{1}{Re}\left(\frac{\partial^2 V_p}{\partial X^2} + \frac{\partial^2 V_p}{\partial Y^2}\right) - \frac{1}{Re\, Da}\varepsilon V_p - \frac{F|\vec{u}_p|}{\sqrt{Da}}\varepsilon V_p \tag{17}$$

energy equation

$$U_p\frac{\partial\theta_p}{\partial X}+V_p\frac{\partial\theta_p}{\partial Y}=\frac{\partial}{\partial X}\left(\frac{1}{Re\,Pr_p}\frac{\partial\theta_p}{\partial X}\right)+\frac{\partial}{\partial Y}\left(\frac{1}{Re\,Pr_p}\frac{\partial\theta_p}{\partial Y}\right) \tag{18}$$

(3) Boundary conditions
on surface AB (symmetrical line)

$$U_f=0\frac{\partial V_f}{\partial X}=0\frac{\partial\theta_f}{\partial X}=0$$

$$\text{and}\quad U_p=0\frac{\partial V_p}{\partial X}=0\frac{\partial\theta_p}{\partial X}=0 \tag{19}$$

on surface BC (heated region)

$$U_p=0\,V_p=0\,\theta_p=1 \tag{20}$$

on surface CD (insulated region)

$$U_f=0\,V_f=0\frac{\partial\theta_f}{\partial Y}=0 \tag{21}$$

on surface ED ($X\to\infty$)

$$\frac{\partial U_f}{\partial X}=0\frac{\partial V_f}{\partial X}=0\frac{\partial\theta_f}{\partial X}=0 \tag{22}$$

on surface EF ($Y\to\infty$)

$$\frac{\partial U_f}{\partial Y}=0\frac{\partial V_f}{\partial Y}=0\frac{\partial\theta_f}{\partial Y}=0 \tag{23}$$

on surface FG (wall)

$$U_f=0\,V_f=0\frac{\partial\theta_f}{\partial X}=0 \tag{24}$$

on surface GA (jet inlet)

$$U_f=0\,V_f=-1\,\theta_f=0. \tag{25}$$

There are some interfacial conditions at the interfaces between the porous block and the external flow field. These are the matching conditions of the horizontal and vertical velocities, normal and shear stresses, temperature, heat flux, and pressure. However, these conditions will make the problem more complex. A simplified method suggested to solve these interfacial problems was discussed in the study of Hadim [3]. The interfacial conditions at the fluid–porous medium interface are automatically satisfied [3] due to the Brinkman extension in the momentum equation of the porous media.

NUMERICAL METHOD

The SIMPLEC algorithm [17] with TDMA solver [18] is used to solve the governing equations (11)–(18) for the flow and thermal fields. Equations (11)–(18) are first discretized into algebraic equations by using the control volume method [18] with a power-law scheme. The underrelaxation factor is 0.3 for both the velocity and the temperature field. The conservation residues [17] of the momentum, energy and continuity equations, and the relative errors of each variable, are used to examine the convergence criteria which are defined as follows:

$$(\Sigma|\text{residue of }\Phi\text{ equation}|_{cv}^2)^{1/2}\leqslant 10^{-4}$$

$$\Phi=U,V,\theta\text{ and mass flow rate} \tag{26}$$

$$\frac{\max|\Phi^{n+1}-\Phi^n|}{\max|\Phi^{n+1}|}\leqslant 10^{-5}\quad\Phi=U,V,P\text{ and }\theta. \tag{27}$$

In order to reduce the computation time, a non-staggered mesh is used. The finer meshes are placed in both the interfacial region of the porous block and near the solid wall region. The meshes are then expanded outwards from the interfacial boundary and the solid wall with a scale ratio of 1.05. Due to the limitations of the numerical method, the inclined interfacial surfaces of the convex and concave blocks are simulated by a series of rectangular steps, called the 'blocking off' operation, as proposed by Pantankar [18]. For the interfacial control element, if the central position of the control element is lower than the corresponding inclined surface, the control element then belongs to the porous block: otherwise, the control element belongs to the external flow field. In addition, on the basis of the suggestions of Pantankar [18], the harmonic mean formulation of thermophysical properties is used to avoid the effects of an abrupt change in these properties across the interfacial region of the porous block and the external flow field on the computational accuracy.

The parameters, which include the Reynolds number Re, block sizes HP_r and HP_c, and effective porosity ε_e, adopted in this study are tabulated in Table 1. The Darcy number Da listed in Table 1 is based on the effective porosity ε_e. Since the porosity ε is a variable, as shown in equation (1), the Da in each control volume is also a variable during the computation. As for the results of Martin [7] and Gardon and Akfirat [9], the presence of a pressure gradient plays an important role in the value of the local heat transfer coefficient,

Table 1. Main parameters and empirical constants for $\varepsilon_e=0.5$

b [m]	Re	LP	HJ	HP_r, HP_c	d_p [m]	Da	Pr	ε_e	r_1	r_2	D_T	ω
0.01	450	2	3.5	0.125, 0.25, 0.5, 1.0, 1.5, 2.0, 2.5	1.25×10^{-3}	5.208×10^{-3}	0.7	0.5	0.98	2	0.3	3.5

as it could be found that the value of the local static pressure (or local Sherwood number) for the impinging flow for the low jet-to-plate distance and low Reynolds number in this study are almost constant for X larger than 2. Polat *et al.* [13] also mentioned that the range of the impingement region is about 0.5 times that of the jet-to-plate distance for a single jet and non-interacting multiple jets. Therefore, a constant dimensionless ratio of the length of the porous block to the jet width LP is selected and fixed at 2, as listed in Table 1. For the $Re = 450$ cases, the whole dimensionless domain $X \times Y$ is 25.5×12.0, and the fully developed conditions in the outlet sections can be satisfied.

Table 1 also shows the empirical constants used in the definitions of the porosity ε [equation (1)] and the Van Driest's wall function l [equation (10)], where r_1 and r_2 are obtained from Vafai [15], and D_T and ω are provided by Cheng and Hsu [14].

The numerical method and accuracy are validated in Fu *et al.* [6]. After the results of the grid tests, 86×182 meshes are typically chosen for a rectangular block with $Re = 450$, $HP = 0.5$, $HJ = 3.5$, $\varepsilon_e = 0.5$ and $Pr = 0.7$.

RESULTS AND DISCUSSION

The material of the spherical bead adopted in this study is considered to be copper in order to enhance the thermal performance. $Re = 450$, $\varepsilon_e = 0.5$, $Pr = 0.7$, and $HJ = 3.5$ are fixed in the following situations.

In order to illustrate the flow and thermal fields more clearly, only the phenomena near the impingement region are presented. The dimensionless stream function ψ is defined as

$$U = \frac{\partial \psi}{\partial Y} \text{ and } V = -\frac{\partial \psi}{\partial X}. \tag{28}$$

Shown in Fig. 3(a)–(f) are the streamlines and isotherms for the rectangular ($HP_c = HP_r$) porous block

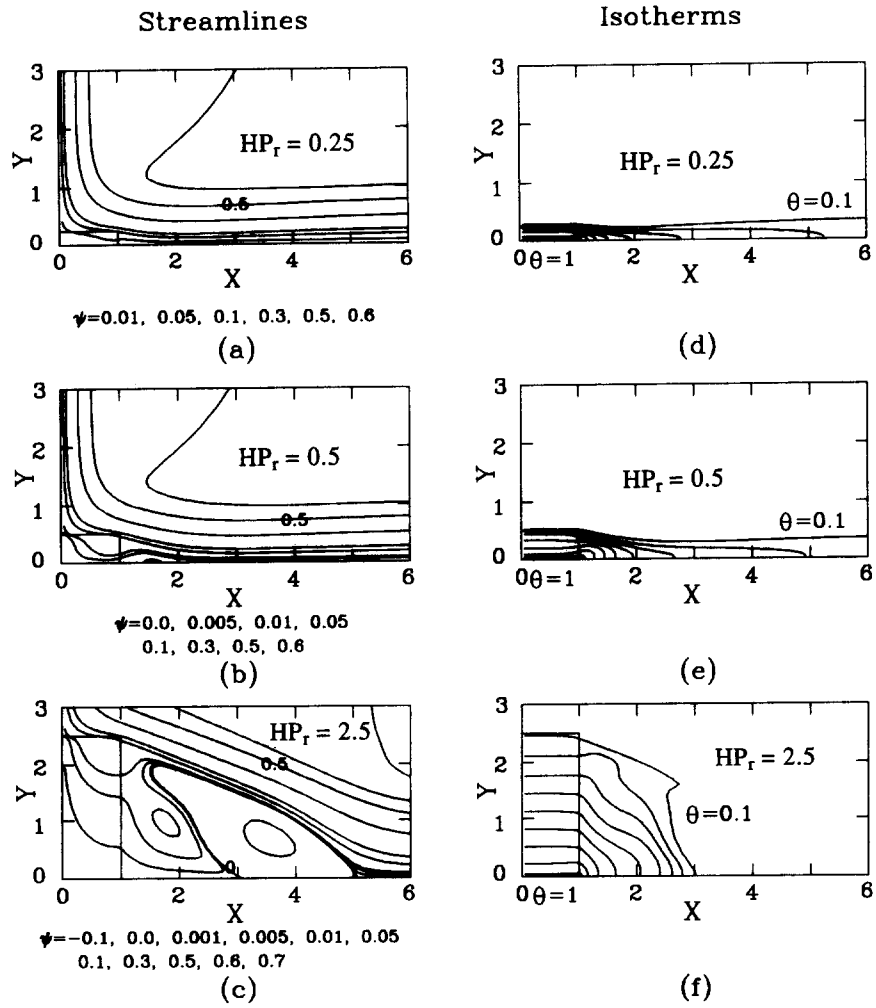

Fig. 3. Streamlines and isotherms for rectangular porous blocks with $Re = 450$, $HJ = 3.5$, $\varepsilon_e = 0.5$, and $Pr = 0.7$: streamlines (a) $HP_r = 0.25$, (b) $HP_r = 0.5$, and (c) $HP_r = 2.5$, and isotherms (d) $HP_r = 0.25$, (e) $HP_r = 0.5$, and (f) $HP_r = 2.5$.

Table 2. Ratio of flow rate ($\dot{m}_p$) of fluid penetrating a porous block to that at the jet inlet ($\dot{m}_o$)

HP Shapes	0.125	0.25	0.5	1.0	1.5	2.0	2.5
				$\dot{m}_p/\dot{m}_o$			
Rectangular block ($HP_r = HP_c = HP$)	0.066	0.109	0.153	0.180	0.188	0.191	0.192
Convex block ($HP_c = HP$, $HP_r = 0$)	0.050	0.115	0.231	0.354	0.418	0.426	0.432
Concave block ($HP_r = HP$, $HP_c = 0$)	0.075	0.145	0.250	0.382	0.477	0.576	0.666

cases for $HP_r = 0.25$, 0.5 and 2.5. The smaller the HP_r, the lower is the height of the block. As the value of HP_r increases, the porous block moves closer to the jet and the fluid flow through the porous block increases gradually, as indicated in Table 2. In addition, as the height of the porous block increases, a circulation region near the right-hand side of the porous block grows. This flow pattern damages the heat transfer performance of the heated region.

As the value of HP_r increases, the isotherms are distributed evenly in the porous block. Due to the existence of the circulation region next to the right-hand side of the block when $HP_r = 2.5$, the isotherms are distributed around the low right corner, and cannot extend far away. Conduction heat transfer is dominant in the porous block.

As indicated in Table 2, $\dot{m}_p$ is the flow rate of a fluid penetrating the porous block, and $\dot{m}_o$ is the flow rate of a fluid at the jet inlet. Only a small portion of the fluid can penetrate the rectangular porous block, as shown in Table 2. The higher the HP_r, the more fluid penetrates the block. However this phenomenon does not simultaneously guarantee that more fluid can flow near the heated region, which is advantageous for the heat transfer from the heated region. Figure 4(a)–(c) shows the distribution of velocity U along the Y-direction near the heated region. The symbol '+' in Fig. 4 is the location of the interfacial surface of the porous block. The velocities are small in the heated region of the higher block cases ($HP_r = 1.5$ and 2.5): meanwhile, a channeling effect is hardly found for the velocity distribution. From a heat transfer point of view, the higher blocks ($HP_r = 1.5$ and 2.5) are regarded as a barrier in spite of more fluid penetrating the block. Shown in Fig. 5(a)–(f), are streamlines and isotherms for the convex ($HP_c \geqslant HP_r$, $HP_r = 0$) porous block cases ($HP_c = 0.25$, 0.5 and 2.5). The inclined surface of the block looks like a simulated flow streamline. Since the shape of the convex block is more streamlined than that of the rectangular block mentioned above, the circulation region becomes smaller for a larger value of HP_c. As for the distribution of the isotherms, the trends in the isotherms are like those for the rectangular blocks shown in Fig. 3, except for the situation when $HP_c = 2.5$. The isotherms are prolonged farther downstream in the $HP_c = 2.5$ case, which is advantageous for the heat transfer performance.

The flow rage $\dot{m}_p$ of fluid penetrating the convex block is listed in Table 2. The same trend appears for the rectangular case. For most of the cases, the flow

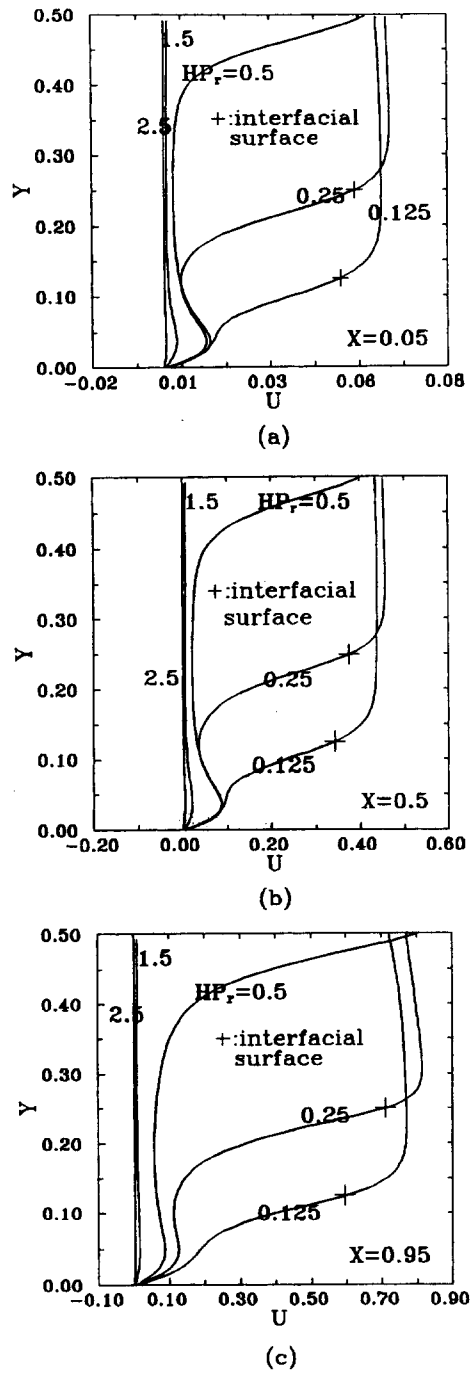

Fig. 4. Distributions of velocity U along the Y-direction for the rectangular porous block at: (a) $X = 0.05$, (b) $X = 0.5$, and (c) $X = 0.95$.

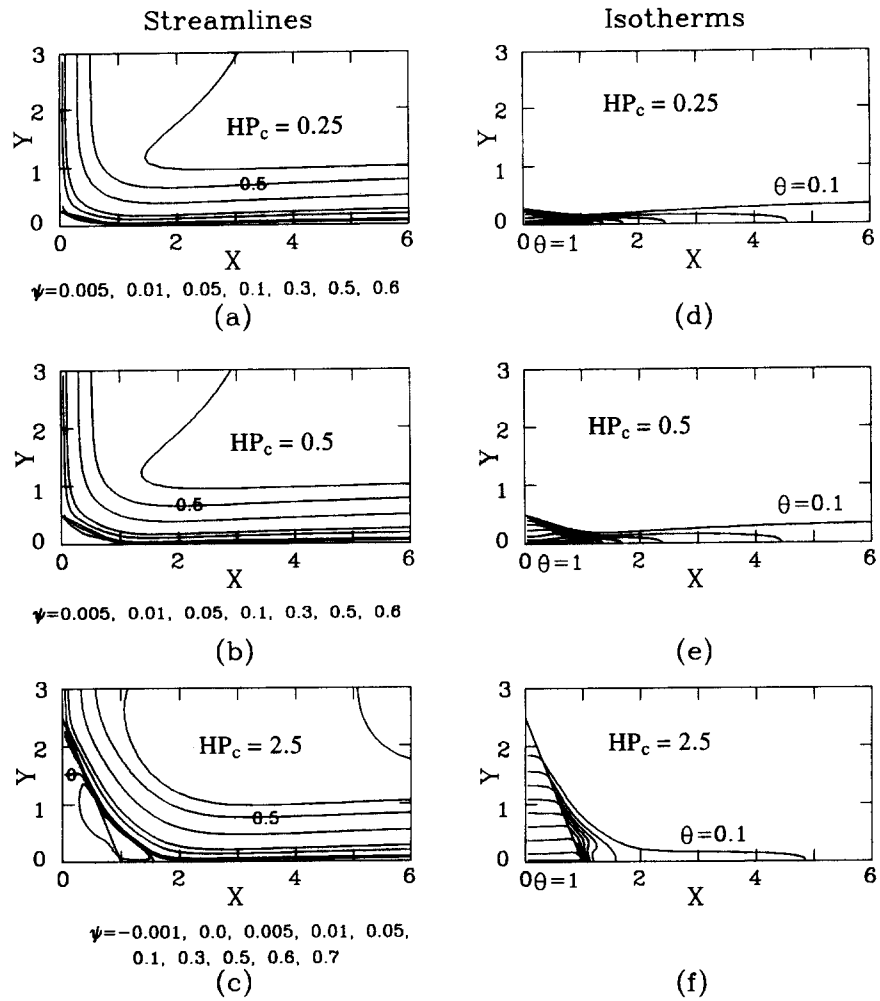

Fig. 5. Streamlines and isotherms for convex porous blocks with $Re = 450$, $HP_r = 0$, $HJ = 3.5$, $\varepsilon_e = 0.5$, and $Pr = 0.7$: streamlines (a) $HP_c = 0.25$, (b) $HP_c = 0.5$, and (c) $HP_c = 2.5$, and isotherms (d) $HP_c = 0.25$, (e) $HP_c = 0.5$, and (f) $HP_c = 2.5$.

rate $\dot{m}_p$ for the convex block is greater than that for the rectangular type, except for the $HP_c = 0.125$ case.

In Fig. 6(a)–(c), the fluid is hardly able to flow near the heated region for $HP_c = 1.5$ and 2.5. The central region is thicker than the right-hand region, which causes the fluid velocity to increase near the right-hand region, and the channeling effect is observed only in a few cases ($HP_c = 0.25$ and 0.5 at $X = 0.05$, and $HP_c = 0.5$ at $X = 0.5$). Figure 6(c) illustrates that some fluids are induced to penetrate the block from the external flow near the right-hand region for $HP_c = 1.5$ and 2.5.

For the concave ($HP_c \leqslant HP_r$, $HP_c = 0$) porous blocks, the streamlines and isotherms are presented in Fig. 7(a)–(f) for $HP_r = 0.25$, 0.5 and 2.5. In Fig. 7, due to the shape of the block, the fluids are easily induced to flow into the cavity formed by the concave block, which causes more fluid to flow away from the block through the right-hand surface. As a result, a circulation region no longer exists near the block. This phenomenon is helpful for the heat transfer performance of the heated region. Since more fluid flows through the concave block, as listed in Table 2, the convective heat transfer becomes dominant, which results in the isotherms no longer being distributed evenly in the block, even in the situation of the larger value of HP_r. The isotherms extend farther in the downstream direction.

As shown in Fig. 8(a)–(c), the channeling effect is remarkable for $HP_r = 1.5$ and 2.5, which is opposite to the two blocks mentioned above. However, for $HP_r = 0.125$, 0.25 and 2.5, the channeling effect is observed near the right-hand region ($X = 0.95$) and not near the central region ($X = 0.05$). The phenomena are also contrary to those for the two blocks mentioned above.

Fig. 9 illustrates the effects of HP on the thermal performances of the above three types of porous block. The mean Nusselt numbers for the block and

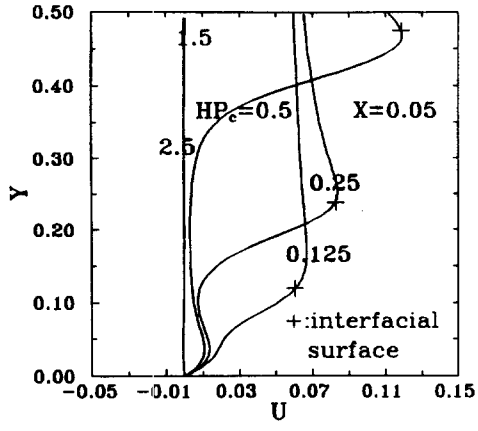

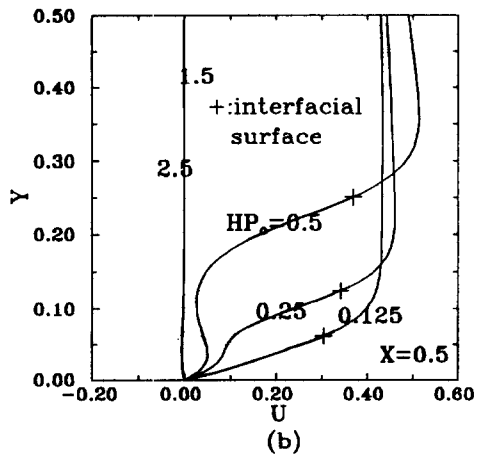

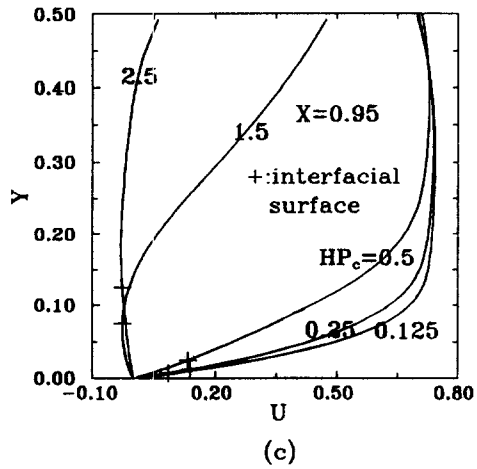

Fig. 6. Distributions of velocity U along the Y-direction for the convex porous block at: (a) $X = 0.05$, (b) $X = 0.5$ and (c) $X = 0.95$.

the without-porous-block case are $\overline{Nu_p}$ and $\overline{Nu_{wop}}$, respectively, and are defined as

$$\overline{Nu_p} = \frac{1}{LP}\int_0^{LP}\left(-\frac{k_e\partial\theta_p}{k_f\partial Y}\right)\Big|_{Y=0} dX \qquad (29)$$

$$\overline{Nu_{wop}} = \frac{1}{LP}\int_0^{LP}\left(-\frac{\partial\theta_f}{\partial Y}\right)\Big|_{Y=0} dX. \qquad (30)$$

The ratio of the $\overline{Nu_p}$ to $\overline{Nu_{wop}}$ indicates enhancement of the heat transfer performance. For a small value of HP ($HP < 0.25$), fluids easily flow near the heated region, and the contact surface between the porous medium and the fluid effectively executes heat transfer performance. For all three types of porous block, the $\overline{Nu_p}$ values for the $HP = 0.125$ case are smaller than those for the $HP = 0.25$ case. In this study, the number of beads in the Y-direction for the $HP = 0.125$ and 0.25 cases is only 1 and 2, respectively, which causes the difference in the flow resistance for both cases to be small, and the flow patterns for these two cases are not significantly different. However, the contact surface between the porous medium and the fluid for the $HP = 0.25$ case is larger than that for the $HP = 0.125$ case. Consequently, the values of $\overline{Nu_p}$ for the $HP = 0.125$ cases are slightly smaller than those for the $HP = 0.25$ cases. Therefore, the maximum values of the mean Nusselt number exist for all three blocks, and about 20% enhancement is achieved.

As the value of HP increases, the block gradually becomes a barrier for the fluid flowing near the heated region, in spite of the enlargement of the contact surface between the porous medium and the fluid, which results in the mean Nusselt number being small. As a result, the value of the ratio of $\overline{Nu_p}$ to $\overline{Nu_{wop}}$ is even smaller than those for the larger HP cases of the rectangular and convex porous cases. Since more fluid flows through the concave block, the mean Nusselt number for the concave block is larger than those for the convex and rectangular blocks.

The concave porous block is recognized from the above discussion as effective for enhancing the heat transfer performance. Therefore, only the effects of HP_c for the concave porous block on the $\overline{Nu_p}$ are illustrated in Fig. 10 for $HP_r = 0.25$, 0.5, 1.0 and 1.5. Each line shows the variation in $\overline{Nu_p}/\overline{Nu_{wop}}$ with HP_c/HP_r varying from 0 to 1. When the value of HP_c is small, the fluid easily flows near the heated region, and the contribution of the contact surface to the heat transfer is dominant, the value $\overline{Nu_p}/\overline{Nu_{wop}}$ increases as HP_c increases: after that, the contribution of the contact surface is gradually reduced. The value of $\overline{Nu_p}/\overline{Nu_{wop}}$ then decreases with increasing HP_c.

In Fig. 11, the effects of the distance HZ from the inlet of the jet to the plate on the mean Nusselt number for the concave porous blocks are presented. The conditions for $\overline{Nu_{wop}}$ are the same as in the previous discussion. For the dashed line, the distance HZ is fixed and the HJ is variable: for the solid line, the distance HZ is variable and the distance HJ is fixed and equal to 3.5. For $HP_r \leqslant 1.0$, the block is comparatively small, which causes the flow resistance to be small: both two situations then have the same mean Nusselt number. After that, as HP_r increases, the different behavior of both situations becomes apparent. For the case of $HZ = 3.5$ (dashed line), increasing HP_r

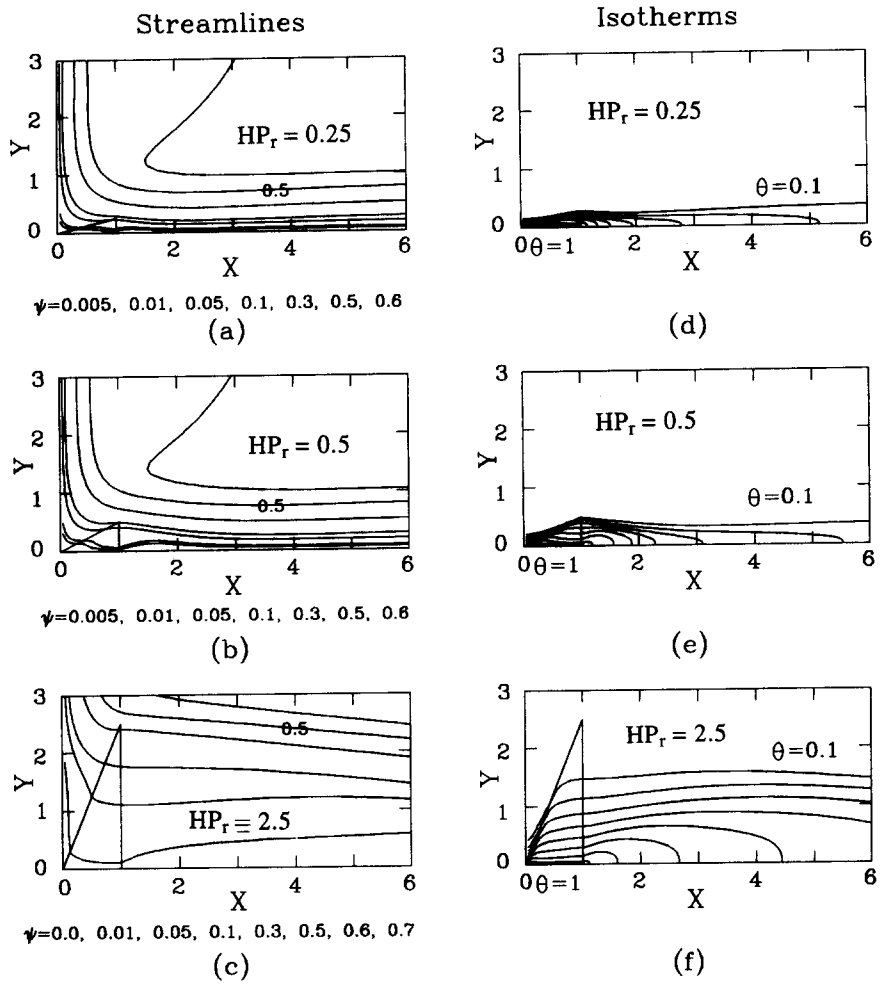

Fig. 7. Streamlines and isotherms for concave porous blocks with $Re = 450$, $HP_c = 0$, $HJ = 3.5$, $\varepsilon_e = 0.5$, and $Pr = 0.7$: streamlines (a) $HP_r = 0.25$, (b) $HP_r = 0.5$, and (c) $HP_r = 2.5$, and isotherms (d) $HP_r = 0.25$, (e) $HP_r = 0.5$, and (f) $HP_r = 2.5$.

means that the porous block is closer to the jet inlet. Therefore, more fluid penetrates the porous block and enhances the heat transfer performance. Hence, $\overline{Nu}_p$ increases as the HP_r increases.

CONCLUSIONS

The thermal performance of a porous block mounted on a heated region with a laminar slot impinging jet is studied numerically. Three different types (rectangular, convex and concave) of porous blocks are considered. The results can be summarized as follows:

(1) For a lower porous block, the heat transfer is enhanced by three types of porous blocks. However, for a higher porous block, heat transfer is only enhanced by the concave porous block.

(2) The heat transfer performance of a heated region is mainly affected by the flow rate of fluid near the heated region.

Acknowledgements—The support of this work by National Science Council, Taiwan, Republic of China under contract NSC86-2212-E-009-042 is gratefully acknowledged.

REFERENCES

1. Vafai, K. and Kim, S. J., Analysis of surface enhancement by a porous substrate. *Journal of Heat Transfer*, 1990, **112**, 700–706.
2. Huang, P. C. and Vafai, K., Flow and heat transfer control over an external surface using a porous block array arrangement. *International Journal of Heat and Mass Transfer*, 1993, **36**, 4019–4032.
3. Hadim, A., Forced convection in a porous channel with localized heat sources. *Journal of Heat Transfer*, 1994, **116**, 465–472.
4. Huang, P. C. and Vafai, K., Analysis of forced convection enhancement in a channel using porous blocks. *AIAA Journal of Thermophysics and Heat Transfer*, 1994, **8**, 563–573.
5. Hwang, G. J. and Chao, C. H., Heat transfer measurement and analysis for sintered porous channels. *Heat and Mass Transfer in Porous Media*, 1992, HTD-Vol. 216, 19–26.
6. Fu, W.-S., Huang, H.-C. and Liou, W.-Y., Thermal

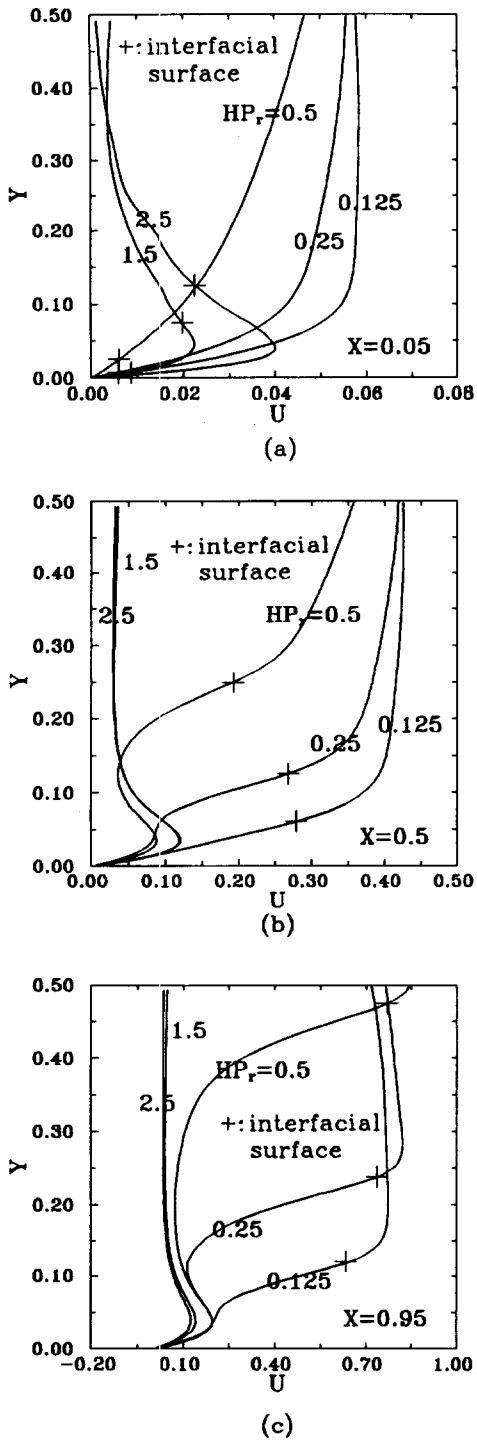

Fig. 8. Distributions of velocity U along the Y-direction for the concave porous block at: (a) $X = 0.05$, (b) $X = 0.5$, and (c) $X = 0.95$.

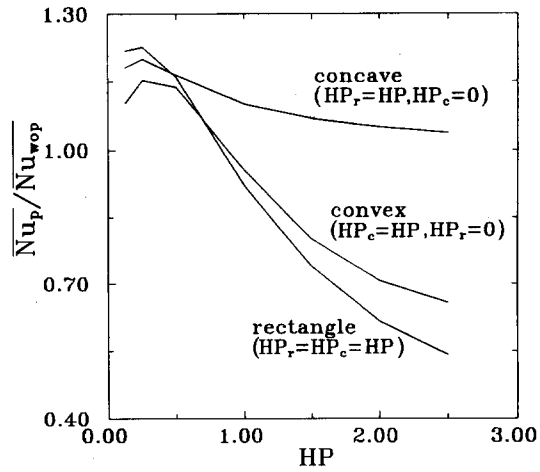

Fig. 9. Mean Nusselt number distributions for rectangular, convex, and concave porous blocks with $Re = 450$, $HJ = 3.5$, $\varepsilon_e = 0.5$, and $Pr = 0.7$.

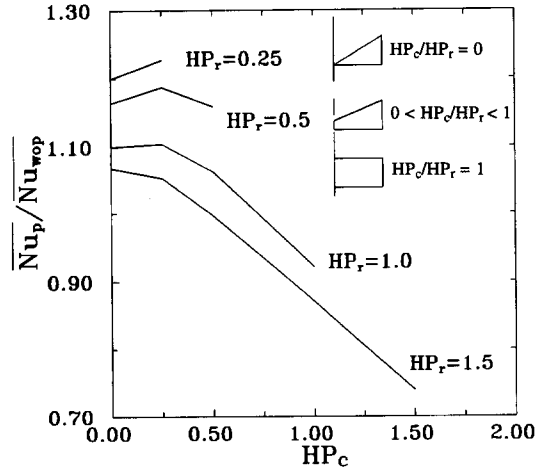

Fig. 10. Effects of HP_c on the mean Nusselt number for different HP_r concave porous blocks with $Re = 450$, $HJ = 3.5$, and $Pr = 0.7$.

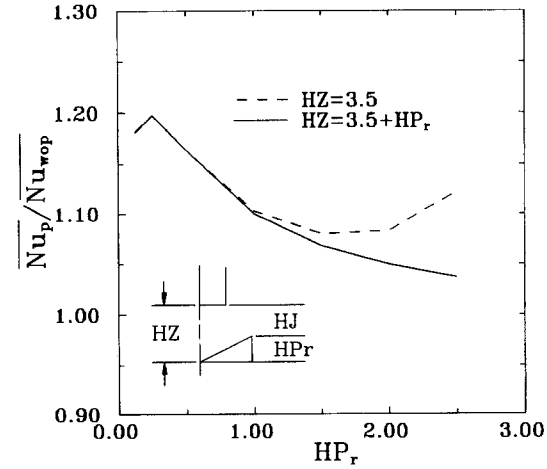

Fig. 11. Effects of HZ on the mean Nusselt number for different HP_r concave porous blocks with $Re = 450$, $HP_c = 0$, $\varepsilon_e = 0.5$, and $Pr = 0.7$.

enhancement in laminar channel flow with a porous block. *International Journal of Heat and Mass Transfer*, 1996, **39**, 2165–2175.
7. Martin, H., Heat and mass transfer between impinging gas jets and solid surface. *Advances in Heat Transfer*, 1977, **13**, 1–60.
8. Gardon, R. and Akfirat, J. C., The role of turbulence in determining the heat-transfer characteristics of impinging jets. *International Journal of Heat and Mass Transfer*, 1965, **8**, 1261–1271.
9. Gardon, R. and Akfirat, J. C., Heat transfer characteristics of impinging two-dimensional air jets. *Journal of Heat Transfer*, 1966, **88**, 101–108.
10. Miyazaki, H. and Silberman, E., Flow and heat transfer on a flat plate normal to a two-dimensional laminar jet issuing from a nozzle of finite height. *International Journal of Heat and Mass Transfer*, 1972, **15**, 2097–2107.
11. Sparrow, E. M. and Lee, L., Analysis of flow field and impingement heat/mass transfer due to a nonuniform slot jet. *Transations of the ASME, Series C, Journal of Heat Transfer*, 1975, **97**, 191–197.
12. Jambunathan, K., Lai, E., Moss, M. A. and Button, B. L., A review of heat transfer data for single circular jet impingement. *International Journal of Heat Fluid Flow*, 1992, **13**, 106–115.
13. Polat, S., Huang, B., Mujimdar, A. S. and Douglas, W. J. M., Numerical flow and heat transfer under impinging jets. *Annual Review of Numerical Fluid Mechanics and Heat Transfer*, Vol. 2. Hemisphere, New York, 1989, pp. 157–197.
14. Cheng, P. and Hsu, C. T., Applications of Van Driest's mixing length theory to transverse, thermal dispersion in a packed-bed with boundary walls. *International Communications in Heat and Mass Transfer*, 1986, **13**, 613–625.
15. Vafai, K., Convective flow and heat transfer in variable-porosity media. *Journal of Fluid Mechanics*, 1984, **147**, 233–259.
16. Hsu, C. T. and Cheng, P., Thermal dispersion in a porous medium. *International Journal of Heat and Mass Transfer*, 1990, **33**, 1587–1597.
17. Van Doormaal, J. P. and Raithby, G. D., Enhancements of the SIMPLE method for predicting incompressible fluid flows. *Numerical Heat Transfer*, 1984, **7**, 147–163.
18. Pantankar, S. V., *Numerical Heat Transfer and Fluid Flows*. Hemisphere, Washington, D.C., 1980.